Local Results Verification of a 3D Non-Linear Lifting Line Method for Fluid-Structure Interactions Simulation on a Towing Kite for Vessels

Chloé Duport, **Mathias Deberque, Jean-Baptiste Leroux, Kostia Roncin, Christian Jochum**,
ENSTA Bretagne IRDL, Brest/France, chloe.duport@ensta-bretagne.org

Abstract

This paper describes a 3D non-linear model based on the lifting line of Prandtl, expanded to address cases of wing with dihedral and sweep angles variable along the span, and with any flight kinematic including translation velocities and turning rates. This model has been checked by comparison with 3D RANSE simulations and shows good consistency with a relative gap of less than 10% for the global lift and drag coefficients on two different geometries. The local aerodynamic forces comparison gives also satisfying results on classical geometries even with various angle of incidence and sideslip.

1. Introduction

The "beyond the sea®" project aims to develop tethered kite systems as ships auxiliary propulsion to reduce fuel consumption with the use of renewable energy. Indeed, *Wellicome and Wilkinson (1984)* showed that kite wings are more effective for wind propulsion than other common systems. The fuel savings can be predicted by *Leloup et al. (2016)*. For the auxiliary propulsion of merchant ships, the common sport kites need a significant upscaling as they can be larger than 300 m². Therefore, it is not possible to experimentally test each new geometry. As the kite is a flexible structure, fluid-structure interaction (FSI) has to be taken into account to calculate the flying shape, *Bosch et al. (2014)*. Knowing the computational time necessary to carry out a fully coupled simulation using Finite Element and Computational Fluid Dynamics methods, it can be very useful in a design phase to use fast and reliable models to estimate rapidly the kite performances. Furthermore, fast simulations allow the studies of different trajectories and the determination of the critical load case, where more complex models can be used.

For the estimation of the kite performance, *Dadd et al. (2010)* use the zero-mass model, which neglects the weights of the kite and the tethers. This model allows the prediction of the kite velocity and the line tension but gives no information about the local loads, which are necessary to FSI simulations. *Gaunaa et al. (2011)* develop an iterative method which couples a Vortex Lattice Method with 2D airfoil data to consider the effects of airfoil thickness and of viscosity. The results are compared with RANSE simulations and show good agreement for cases without much sideslip. Nevertheless, as the kite can have complex trajectories with a non-null turn rate, the method has to be able to manage these different flight cases. The Prandtl lifting line is also a right method for wing performance prediction. As an example, *Graf et al. (2014)* use a non-linear iterative lifting line method to predict the lift and drag of a two-element straight wing for an AC72 catamaran. The comparison with Reynolds Averaged Navier-Stokes Equations (RANSE) simulations shows a good agreement for attached flow regime. A 3D non-linear lifting line model is already introduced in *Duport et al. (2016)* but the local forces estimation of the model has not been checked.

This study first details the 3D non-linear lifting line method which is implemented to manage wings with high dihedral and sweep angles. In section 3, the settings of the RANSE simulations are presented. The last part compiles the results of the simulations with swept or un-swept wings, purely in incidence or with an angle of sideslip.

2. 3D Non-Linear Lifting Line Method

The 3D non-linear lifting line method is based on an extension of the Prandtl's lifting line theory. This extension is intended to address cases of wings with variable dihedral and sweep angles, and

take into account the non-linearity of the lift coefficient. The kite wind is supposed to fly in a given wind $\overrightarrow{V_{RW}}$. The kite velocity $\overrightarrow{V_K}$ or its turn rate $\vec{\Omega}$ can also be taken into account. The finite wing and its wake are represented by a set of horseshoe vortices of different strengths. The aim of the algorithm presented thereafter is to calculate the circulation Γ^i of each horseshoe vortex. Once these strengths are obtained, the local effective flow for each wing section allows local aerodynamic forces and torques calculation along the span of the wing. The numerical iterative solution is taken from *Anderson (2011)*, but the calculation of the local effective angles of incidence is adapted to the cases of wings which are non-straight and non-planar. The horseshoe vortices used for discretization, and calculation of their influences, are for their part derived from *Katz and Plotkin (2001)*.

The wing is divided in a finite number n of plane sections, each one represented by a horseshoe vortex, which consists of six vortex segments. The bound vortex is located at the local quarter chord length, perpendicularly to the plane of the considered section. An example of the discretized model is presented in Fig.1. This leads to a piecewise constant discretization of the lifting line, as it is theoretically required in order to have a correct match between the local lift calculated from the Kutta formula or from the polar of the section. Non-linear polar curves for the 2D section coefficients of lift, drag and moment about the quarter chord point are also supposed to be given with respect to the angle of incidence.

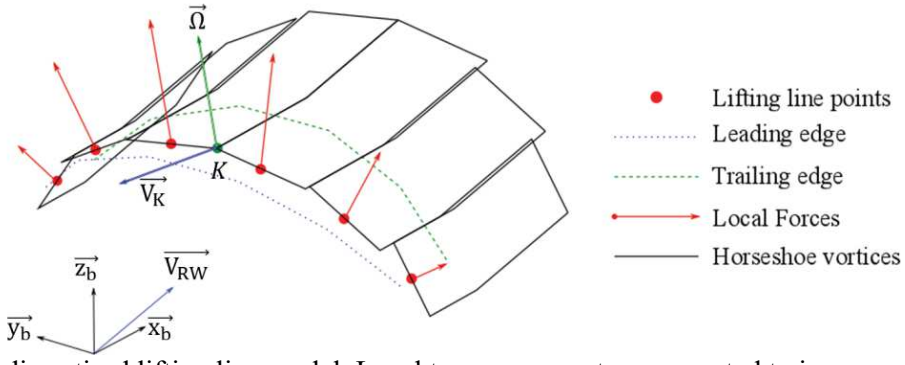

Fig.1: Low discretised lifting line model. Local torques are not reprensented to improve readability

The local circulation values are first initialized by an elliptical distribution along the wing span. Then for each point of the lifting line, the induced velocities by each vortex segment are calculated with the Biot-Savart law and then summed, leading to the induced velocity. The induced velocity combined with the given wind $\overrightarrow{V_{RW}}$, the kite velocity $\overrightarrow{V_K}$ and its turn rate $\vec{\Omega}$ gives the effective wind. This wind is projected in the plane of the section and set the section effective angle of incidence. Using the 2D lift polar curve of the section, the local lift in the section plane can be calculated:

$$L^i = 0.5\rho {V^i_{prj}}^2 c^i C^i_l(\alpha^i_{prj}) \tag{1}$$

With L^i the local lift per unit length, ρ the density of the air, V^i_{prj} the effective wind projected in the plane of the section, c^i the chord length of the section and $C^i_l(\alpha^i_{prj})$ the 2D lift coefficient of the respective section at the effective angle of incidence α^i_{prj}. By construction, this local lift is orthogonal to the effective wind projected in the plane of the section. Therefore, the Kutta formula is equivalent:

$$\vec{L^i} = \rho \overrightarrow{V^i_{eff}} \times \Gamma^i \vec{t^i} \tag{2}$$

With $\overrightarrow{V^i_{eff}}$ the effective wind and $\vec{t^i}$ the normal to the plane section. The new circulation derives from Eq. (1) et (2):

$$\Gamma^i = 0.5 V^i_{prj} c^i C^i_l(\alpha^i_{prj}) \tag{3}$$

The circulation values are finally updated by weighing between the new circulation and the previous

one with a damping factor. This iterative process is repeated until convergence of the circulation distribution.

Once convergence is reached the lift, drag and torque of each section of the wing are then post processed with the converged circulation, which leads to integrated local loads. Finally, these are vectorially summed, to obtain the global force and the global moment about the K point, which apply to the kite wing. The converged result is found to be independent of the initial solution.

Mesh convergence studies were performed. In the cases of straight wings in translation motion parallel to their symmetry plane, very good results versus analytical ones were obtained with at least 10 horseshoe vortices. Nevertheless, in the cases of 3D wings with variable dihedral and sweep, a larger mesh dependency of the converged results was observed, in particular for the total drag coefficient. The mesh having been varied from 10 to 200 sections, the confidence intervals at 95% were estimated using the standard deviations of the results. In the linear range, for angles of incidence typically lower than 10°, it was obtained: 1.0% for the lift, 1.3% for the drag and 1.6% for the moment about the K point. In the non-linear range, for angles of incidence typically greater than 10°, it was obtained: 4.0% for the lift, 15.3% for the drag and 14.1% for the moment about the K point.

3. RANSE simulations settings

The aim of this study is to validate the 3D non-linear lifting line method. For this purpose, 3D RANSE simulations have been performed with the generalist tool STAR-CCM+®. 2D simulations were first used for convergence studies and also to calculate the 2D polar curves of the section, needed in the lifting line model. The parameters of the simulations and the convergence studies are presented in this part.

All the RANSE simulations are incompressible, steady and fully turbulent. The retained turbulence model is the two-equation k-ε realizable model with a two-layer formulation for the wall treatment. The segregated flow solver is based on the SIMPLE algorithm, and a second-order discretization scheme. The kite section or the kite wing is set with respect to the computational domain, to avoid the creation of a new geometry for each calculation case. The direction of the inlet velocity is therefore changed to model the modification of the angle of incidence or the sideslip angle. The chord based Reynolds number is fixed at $3.1 * 10^6$. The turbulence intensity is set to 0.5% and the turbulent viscosity ratio is set to 1.

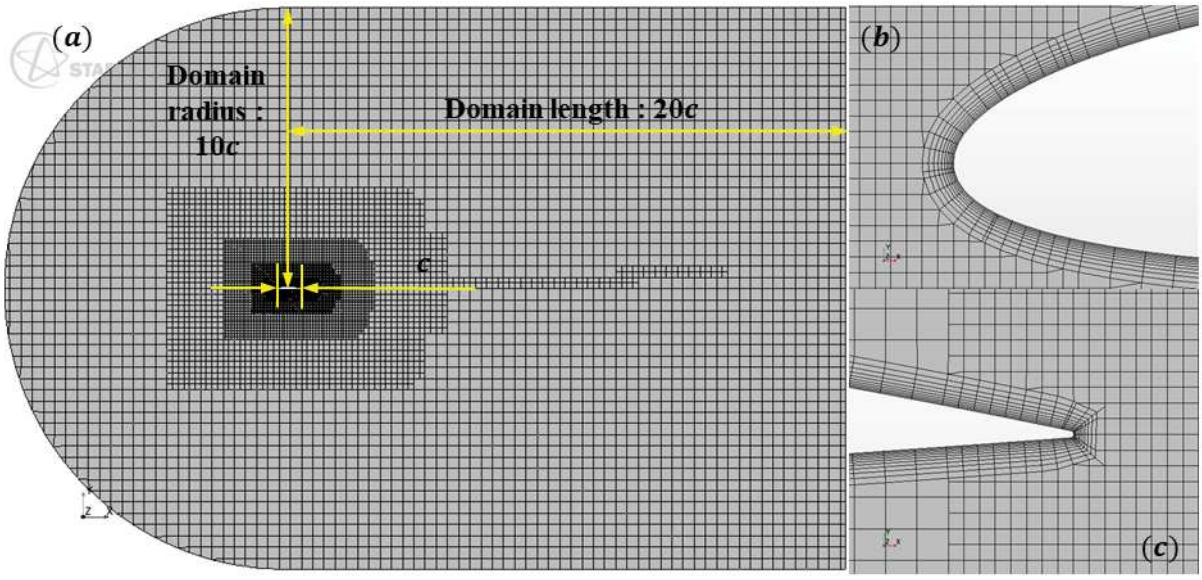

Fig.2: (a) 2D meshed computational domain. (b) Mesh around the profile section. Near wall mesh close to (c) leading edge, (d) trailing edge.

The 2D computational domain is presented Fig.2. The domain is meshed using the trimmed cell mesher, which led to predominantly hexahedral mesh. It is controlled by a cell base size ($0.1c$), with c the chord length of the section, and targeted cell sizes at some boundaries: inlet and outlet ($0.5c$), wing extrados and intrados ($0.025c$), wing leading and trailing edges (0.00625c). The cells size growth rate is very slow, which means at least 8 equal sized cell layer per transition. Around the wing a prism layer mesh is used in order to get orthogonal cells next to the wall. It is controlled by its thickness ($0.0125c$), a number of layer (10) and a growth rate between adjacent cells in the wall normal direction (1.2). Two anisotropic wake refinements are also used in the free stream direction from the trailing edge, one finely meshed (0.00625c) of one chord long and the other coarse ($0.2c$), extending over several chords ($15c$).

In 3D, the same settings are used in addition to a refinement ($0.00625c$) in a conical region at the wing tip, parallel to the mean free stream, in order to partially resolve the tip vortex. The wake refinements are based on the trailing edge and are also parallel to the mean free stream. For the wing with a sweep angle, the same conical refinement is also added at the symmetry plane (see Fig.3). The obtained 2D and 3D meshes are coarse, of about $16 * 10^3$ cells in 2D and $5 * 10^6$ in 3D, and they lead to a mean value of y^+ over the wing surface of about 35 in each simulated case. The stopping criteria of the simulations are based on the monitor of the lift and drag coefficients, specifying a $|max - \min|$ tolerance ever the 10 last calculated values. The tolerance is set to 10^{-6} for both coefficients, and it was found that it corresponds to the fall of the non-dimensional residuals over at least 4 or 5 decades.

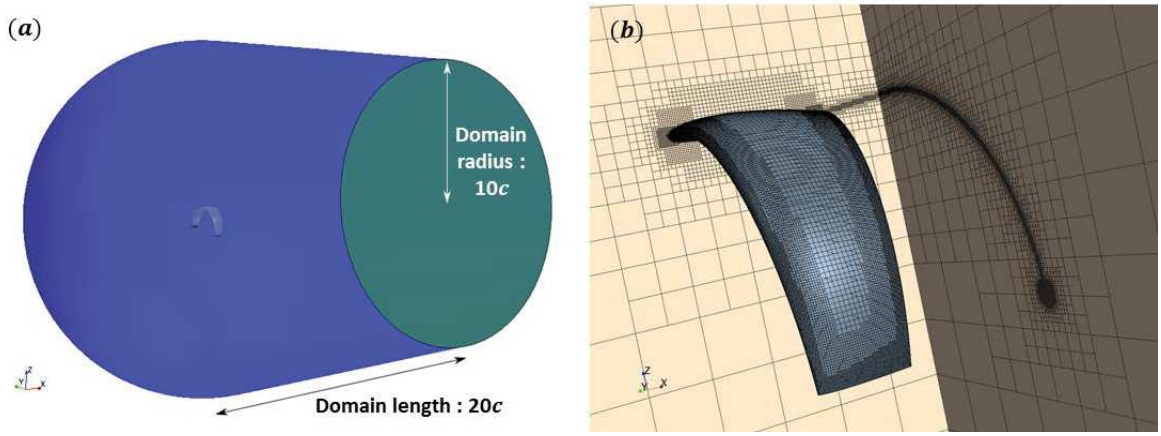

Fig.3: (a) 3D computational domain. (b) 3D mesh with refinements in the wake and near tip vortex

An attempt was done to estimate a numerical accuracy of the 2D and 3D RANSE results. It is supposed that results from 2D simulations are sufficient for that purpose and that they can be extrapolated to 3D cases. In addition, it is assumed sufficient to examine a single angle of incidence of 2° for the root kite section, to be representative.

Three elementary variations of the general numerical set up are considered. The results in term of lift coefficient are presented Fig.4. The obtained curves are similar for the coefficients of drag and moment. First (Fig.4 (a)) the size of the computational domain is varied (parameter N from 1 to 27, domain length=$2Nc$, domain radius=Nc), keeping constant the base size, the absolute targeted sizes at the section, the near wall mesh parameters and the growth rate. Second (Fig.4 (b)) the targeted sizes at each boundary being defined relatively to base size, the base size was varied (from 0.6c to 0.02c, leading to cell count from $6 * 10^3$ to $120 * 10^3$), keeping constant the near wall mesh parameters. Third (Fig.4 (c)) the number of layers of the near wall mesh was varied (from 4 to 32, leading to mean y^+ values from 156 to 0.5), keeping constant all the other mesh parameters. In this last case, two other turbulence models were also tested (k-ω SST and Spalart-Allmaras).

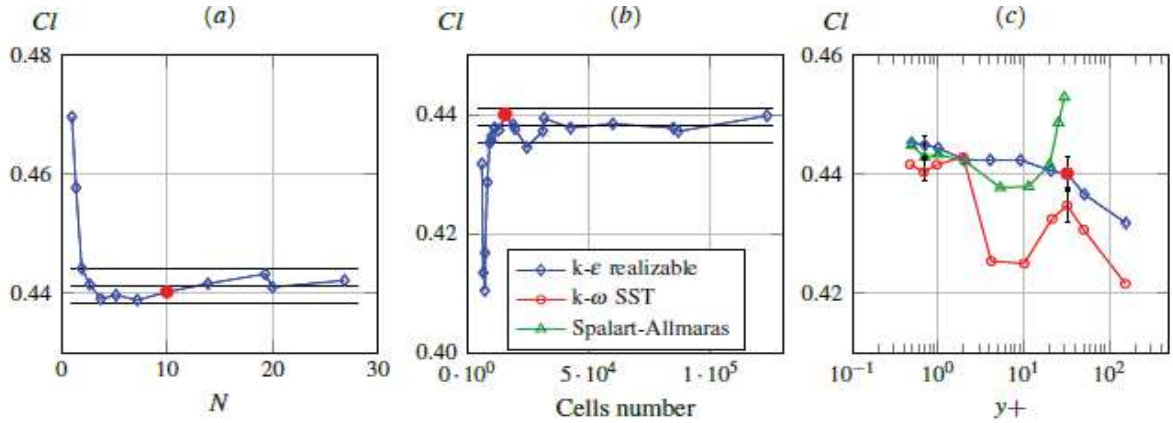

Fig. 4: Convergence history of the lift coefficient for variations (a) of the computational domain size, (b) of the number of cells in the mesh, (c) of the turbulence model and of the number of layers of the near wall mesh

For the variations of the domain size and of the number of cells, based on the limited number of computed points, for each aerodynamic coefficient, it is estimated a mean converged value and a standard deviation relative to this mean, and then a 95% confidence interval. For the variations of the near wall mesh and of the models, respectively around $y^+ \approx 1$ and $y^+ \approx 30$, it is estimated first the coefficients mean values and their standard deviations relative to these means due to model variations, and second the relative difference between coarse and fine mesh mean results. These confidence intervals are plotted in black Fig.4, and it is found that in each case the confidence interval encloses the red filled point corresponding to the general numerical set up presented previously. It can also be noticed Fig.4 (c), as expected, that intermediate meshes in the buffer layer, for y^+ in the range of [5;30], led to highly model dependent results, and that the Spalart-Allmaras model is valid only for fine meshes around y+ = 1.

It is finally estimated that the numerical results provided by the coarse meshed numerical set up presented previously are unconfined, mesh converged, and model independent, with the following relative accuracies: 3.7% for the lift, 7.7% for the drag and 7.1% for the moment.

With this chosen numerical set up, 2D RANSE simulations were carried out on the NACA2412 section for 14 angles of incidence within the range of [-8°;16°]. The numerical results are compared with experimental ones obtained in wind tunnel, *Abbott and von Doenhoff (1959),* at the same Reynolds number. The parametric polar curves used for the lifting line method are established by approaching the RANSE results at best. All these results are presented Fig.5.

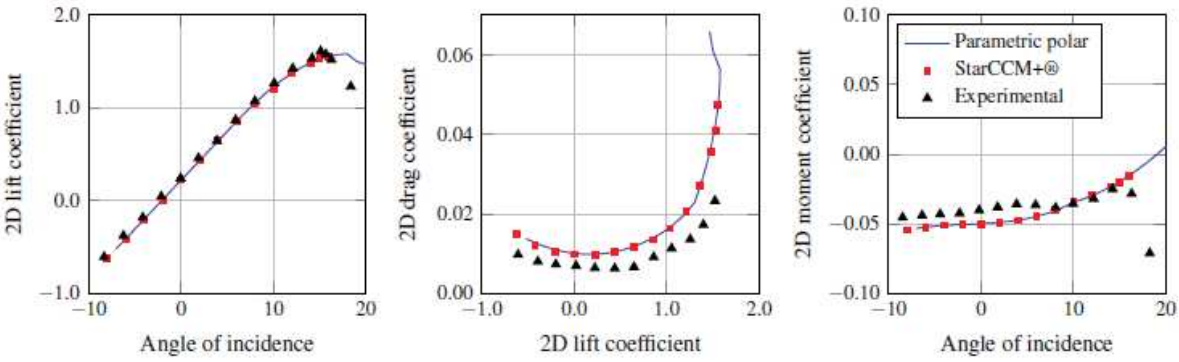

Fig.5: 2D polar curves obtained via StarCCM+®, compared with experimental data, and fitted with parametric polar curves used in the lifting line method

The agreement between experimental and numerical results is excellent for the lift coefficient and satisfactory for the coefficients of drag and of moment. For the last two, one of the explanations for

the differences is that simulations are fully turbulent whereas the experiments were performed on a smooth section in a low residual turbulence wind tunnel.

4. RANSE simulations results

3D RANSE simulations have been performed on a large range of angles of incidence varying between -5° and 16° on two different geometries, one with a sweep angle of 30° and one without. The geometries have also been tested with different sideslip angles (from 0° to 17.5°).

4.1 Un-swept wing

First, the simulations have been carried out on a quite simple geometry. The kite is semi-circular of radius 1.5 m, un-twisted and un-swept. The kite section, defined by the NACA2412 points is kept constant along the span.

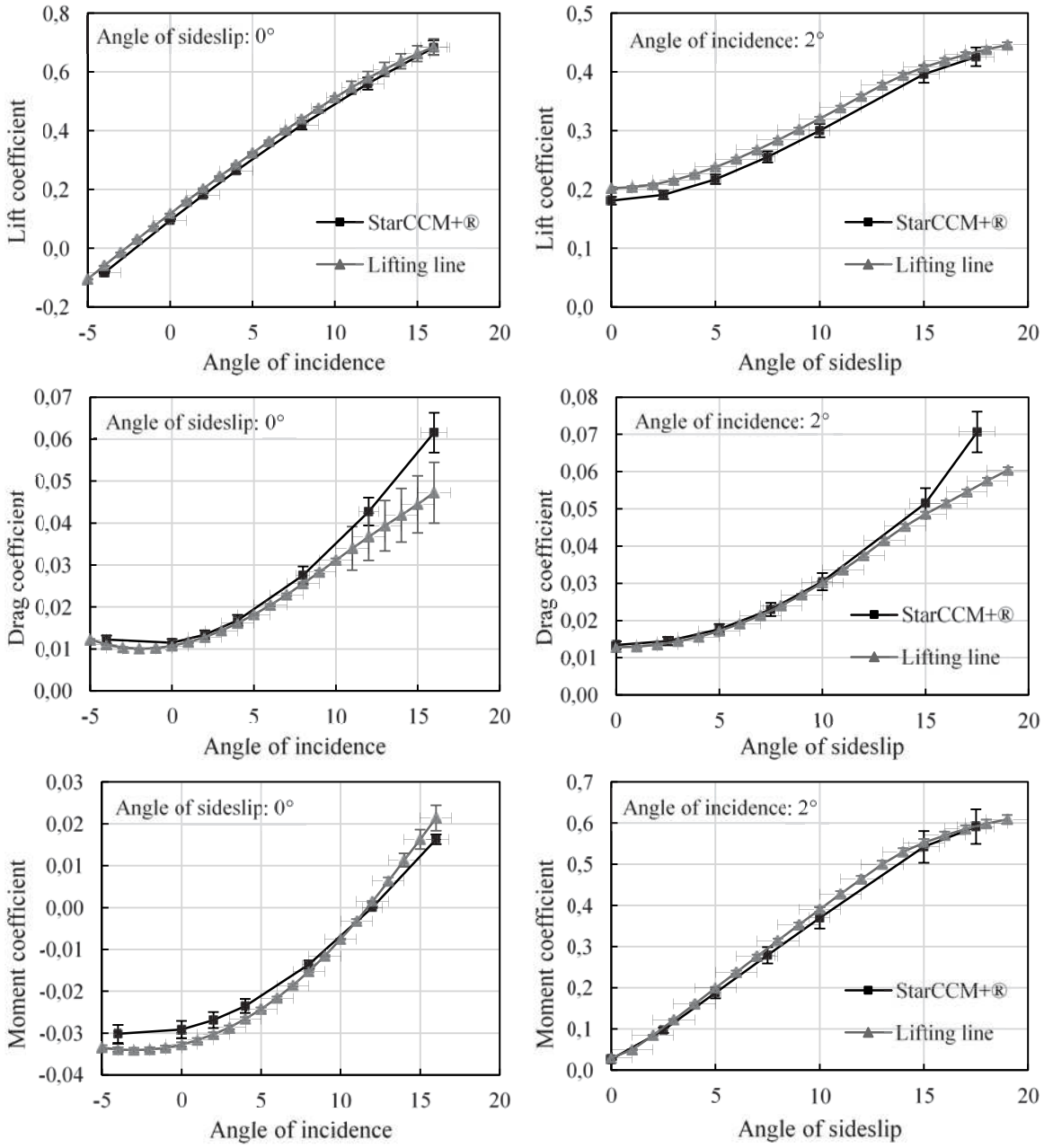

Fig.6: 3D aerodynamic coefficients with respect to the angle of incidence and the angle of sideslip, obtained via StarCCM+® and the lifting line method on a 3D kite.

The chord law varies linearly along the span from 1.0 m at root to 0.5 m at tips. Fig.6 shows the calculated 3D aerodynamic coefficients. The error bars represent the estimated confidence interval at 95% for the RANSE and the lifting line results.

The gap between the two methods purely in incidence is around 5% for the lift coefficient and 12% in average for the moment coefficient. For the drag coefficient, the difference is of 5% at low angle of incidence up to 20% for the higher angle of incidence.

A second set of simulations at 2° of incidence with various angles of sideslip was performed (see Fig.6). The lift coefficient is estimated from the aerodynamic resultant orthogonal to the wind direction. For the lift coefficient, the gap is approximately the same between the kite purely in incidence at 2° and the kite with any sideslip angle included in [0°, 15°] meaning less than 10%. For the drag and moment coefficients, the difference is only of a few percent until 15° of sideslip. With more than 15°, the results for the drag coefficient start to differ significantly.

For the use of the lifting line model in a Fluid-Structure interaction, the local aerodynamic load shall also be validated. On the same geometry without sweep, small slices ($0.025c$) have been added to the RANSE simulations to get the local efforts on the wing. In Fig.7, the magnitude of the local efforts per unit length are presented, nondimensionalized by the maximum local effort of the RANSE simulation. Four simulations have been carried out, three at 2° of incidence with 0°, 7.5° and 15° of sideslip (Fig.7 (a), (b) and (c) respectively), another one at 12° of incidence only (Fig.7 (d)).

The lifting line results are satisfying and follow the same trend than the RANSE simulations, in incidence or in sideslip. The gap is maximum at the center of the kite in incidence and on the most loaded side in sideslip, and always inferior to 15%.

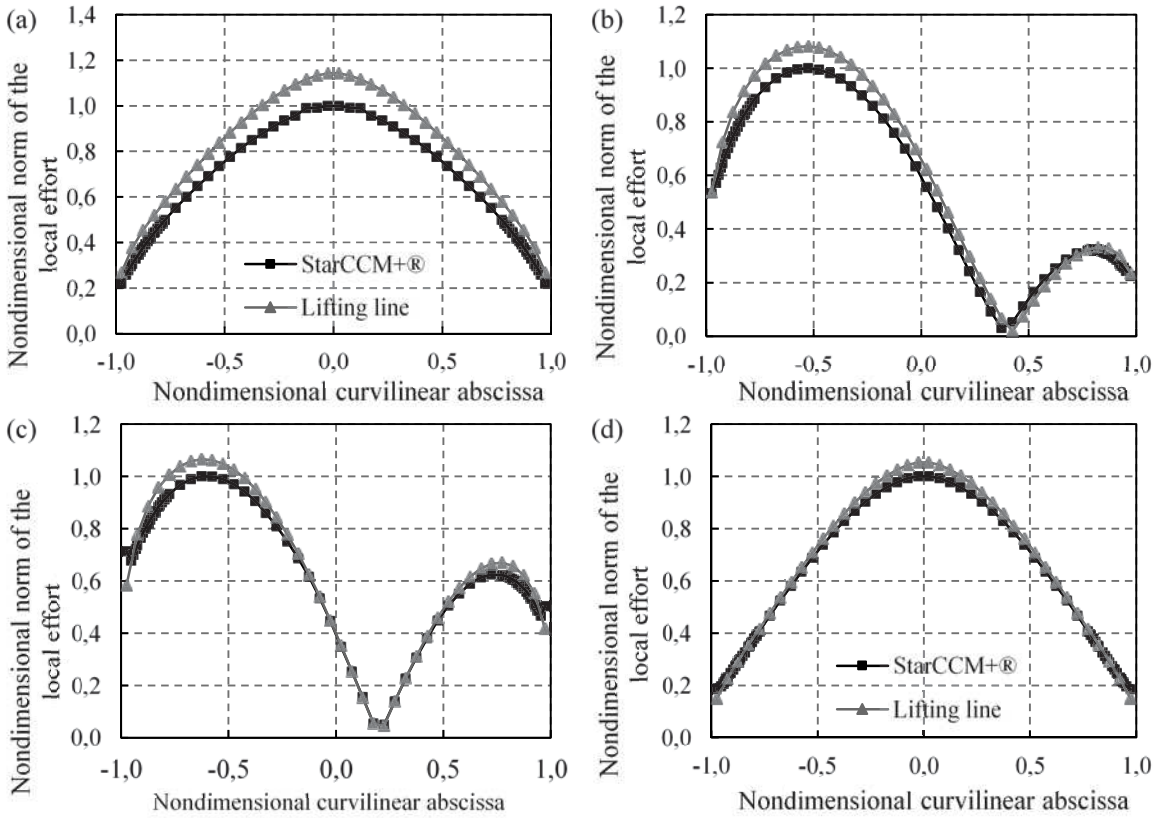

Fig. 7: Nondimensional local aerodynamic force per unit length on a kite wing obtained via StarCCM+® and the lifting line method at 2° of incidence and (a) 0° of sideslip, (b) 7.5° of sideslip, (c) 15° of sideslip, (d) 12° of incidence only.

4.2 High swept wing

To further validate the lifting line model, simulations have been carried out on a swept wing. The geometry is the same than previously described except a linear sweep law of 30° depending on the curvilinear abscissa of the wing. This creates a quite sharp angle at the center of the wing, thus a conical mesh refinement was added to better describe the flow around the center of the kite (see Fig.8).

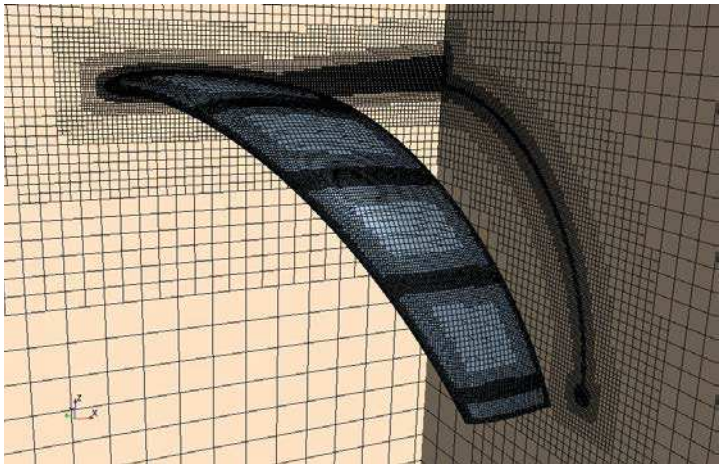

Fig.8: 3D mesh sections with the wake and the two conical refinements. The slices on the wing are also finely meshed.

Fig.9 shows the lift, drag and moment coefficient for the kite purely in incidence. The relative difference between the RANSE results and the lifting line model are around a few percent for the drag coefficient and 9% for the moment coefficient. For the lift coefficient, the relative gap is around 7% with a difference between the two slope coefficients of 10%.

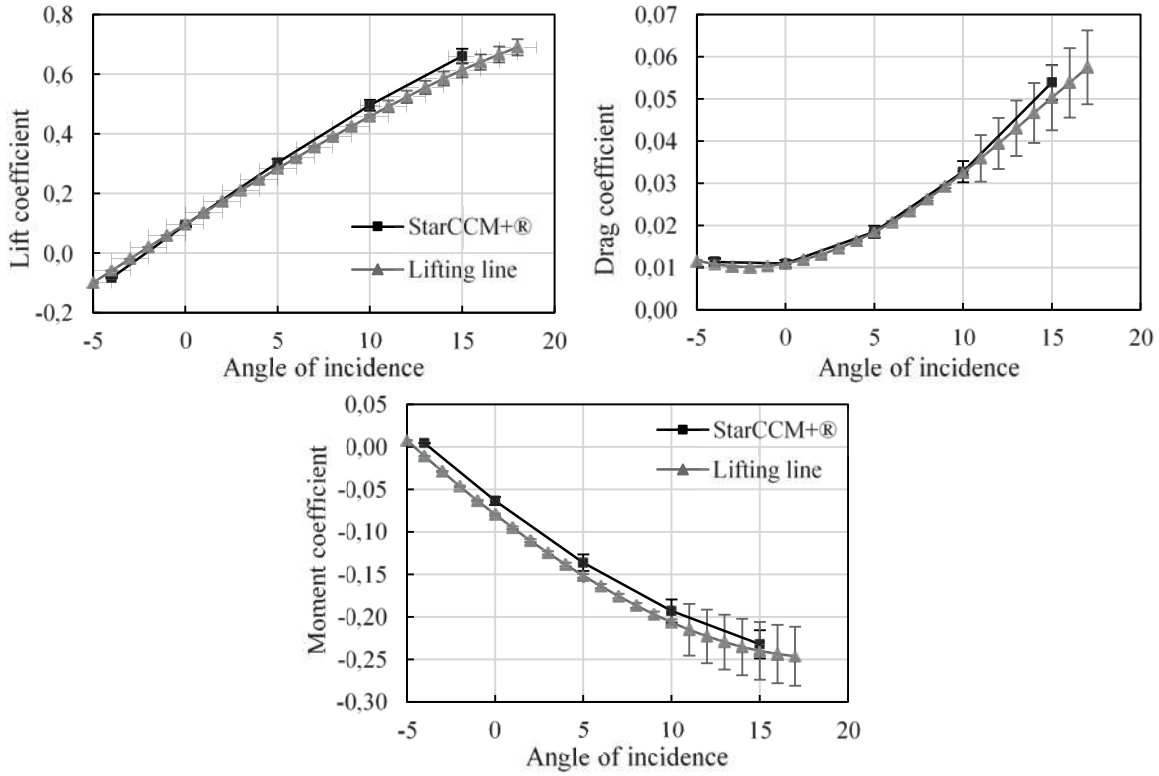

Fig.9: 3D aerodynamic coefficients with respect to the angle of incidence, obtained via StarCCM+® and the lifting line method on a 3D swept kite.

The local aerodynamic efforts have also been computed at -4°, 5° and 15° of incidence. Fig.10 shows as previously the magnitude of the local efforts per unit length nondimensionalized by the maximum local result of the RANSE simulation. The curves show a good consistency at the sides of the kite in contrast with the center of the wing, where the local efforts can differ of almost 60%. These results have to be put in perspective with the fact that the sweep angle is high (30°), therefore the angle in the middle of the wing is sharp. Furthermore, the mesh is coarse ($y^+ = 35$), the RANSE simulations stay diffusive even with the mesh refinement at the center of the kite.

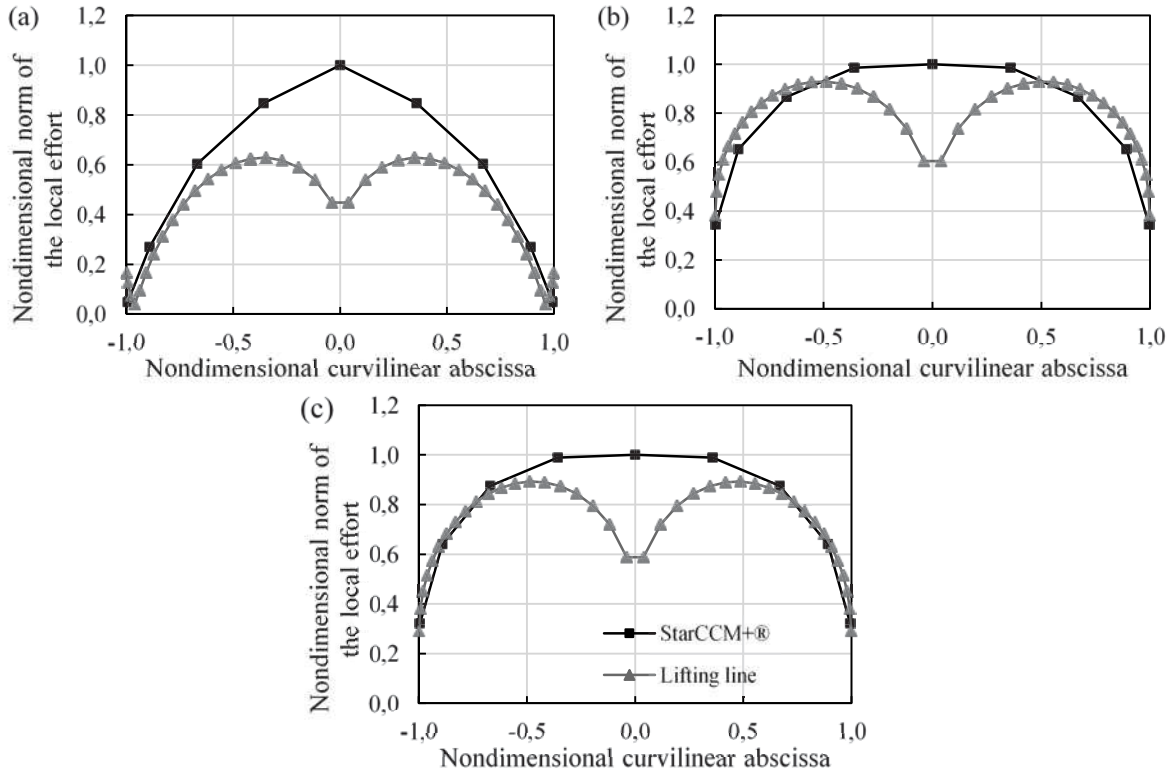

Fig.10: Nondimensional local aerodynamic force per unit length on a swept wing obtained via StarCCM+® and the lifting line at (a) -4°, (b) 5°, (c) 15° incidence angle.

One simulation on the swept wing with a sideslip angle has been carried out. The kite is at 5° of incidence with a sideslip angle of 7.5°. For the global estimation, the gap between the RANSE simulations and the lifting line is of 19% for the lift coefficient and less than 6% for the drag coefficient. The local loads have also been calculated on this swept wing. As can be seen in Fig.11, the two curves follow the same trend with a maximal difference of 10%, except as previously at the center of the wing where the gap reaches 40%.

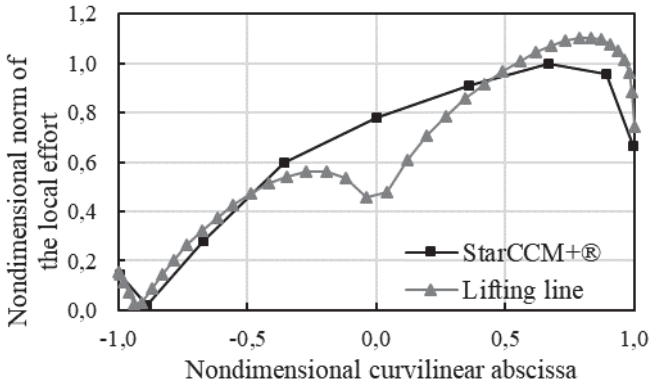

Fig.11: Nondimensional local aerodynamic force per unit length on a swept wing obtained via StarCCM+® and the lifting line method at 5° of incidence and 7.5° of sideslip.

5. Conclusion

A 3D non-linear lifting line model has been described. This iterative model is able to deal with wings, which are non-straight and non-planar, and with high dihedral and sweep angles for any kinematic conditions including kite velocities and turning rates. The method shows a small mesh dependency at low angles of incidence (less than 10°). The results have been checked with 3D RANSE simulations on two different geometries, one un-swept and the other with a high sweep angle of 30°. The global aerodynamic coefficients show good consistency, the lift coefficient estimation is very satisfying in most of the simulation cases with less than 10% of difference between the two methods. The gap for the drag coefficient is only of a few percent at the low angles of incidence and sideslip, up to 20% for the higher angle of incidence. The estimation of the local loads shows also good consistency for the un-swept wing, with the two methods following the same trend even in sideslip. For the swept wing, the local results have to be put in perspective since the mesh of the RANSE simulations is possibly not fine enough to account for the sharp angle of the geometry. Furthermore, the computational efficiency of the lifting line method is indisputable with only a few seconds of computation time.

Acknowledgements

The authors are grateful to the French agency for energy development and control (ADEME) for the funding of this study.

References

ABBOTT, I.H.; DOENHOFF, A.E. von (1959), *Theory of wing sections,* Dover

ANDERSON, J.D. (2011), *Fundamentals of aerodynamics,* McGrawHill, 5th edition

BOSCH, A.; SCHMEHL, R.; TISO, P.; RIWEN, D. (2014), *Dynamic nonlinear aeroelastic model of a kite for power generation,* AIAA J. Guidance, Control and Dynamics, 37(5), pp. 1426-1436, Doi: 10.2514/1.G000545

DADD, G.M.; HUDSON, D.A.; SHENOI, R.A. (2010), *Comparison of two kite force models with experiment,* J. Aircraft, 47(1), pp.212-224

DUPORT, C.; LEROUX, J.-B.; RONCIN, K.; JOCHUM, C. ; PARLIER, Y. (2016), *Comparison of 3D non-linear lifting line method calculations with 3D RANSE simulations and application to the prediction of the global loading on a cornering kite,* 15th Journées de l'Hydrodynamique

GAUNAA, M.; CARQUEIJA, P.; RETHORE, P.-E.; SORENSEN, N. (2011), *A computationally efficient method for determining the aerodynamic performance of kites for wind energy applications,* European Wind Energy Association Conf.

GRAF, K.; HOEVE, A.V.; WATIN, S. (2014), *Comparison of full 3D-RANS simulations with 2D-RANS/lifting line method calculations for the flow analysis of rigid wings for high performance multi-hulls,* Ocean Eng. 90, pp.49-61

KATZ, J.; PLOTKIN, A. (2001), *Low Speed Aerodynamics,* Cambridge University Press

LELOUP, R.; RONCIN, K.; BEHREL, M.; BLES, G.; LEROUX, J.-B.; JOCHUM, C.; PARLIER, Y. (2016), *A continuous and analytical modeling for kites as auxiliary propulsion devoted to merchant ships , including fuel saving estimation*, Renewable Energy 86, pp.483-496

WELLICOME, J.F.; WILKINSON, S. (1985), *Ship propulsive kites; an initial study,* University of Southampton